Cooperation between proximate cell layers drives large-scale wound closure prior to whole-body regeneration

Allison P. Kann and Mansi Srivastava

Department of Organismic and Evolutionary Biology, Museum of Comparative Zoology, Harvard University, Cambridge, MA 02138

Corresponding Author Emails: allisonkann@fas.harvard.edu, mansi@oeb.harvard.edu

KEYWORDS

Regeneration, wound healing, wound closure, morphogenesis

ABSTRACT

Wound healing is a fundamental property of animal life, but the extent to which large injuries can be endogenously repaired varies across phyla. In vertebrates, minor wounds can re-epithelialize on their own, but major wounds often result in imperfect re-epithelialization and fibrotic scarring. In contrast, more regenerative species are capable of both scarless healing and subsequent replacement of missing structures. Due to limitations in many animals' ability to recover from large, multi-tissue injuries, much of our understanding of wound closure comes from experiments studying gaps in epithelial monolayers. In comparison, the mechanisms by which animals can heal large wounds have been characterized primarily at the histological level, usually in non-model species that undergo substantial regeneration after wound healing. Here, we investigate the cellular dynamics of large-scale wound healing in the acoel *Hofstenia miamia*, an invertebrate worm capable of whole-body regeneration. *H. miamia* lack a traditional basement membrane and epidermal cells are not separated from underlying muscle by an organized layer of extracellular matrix - making the system incompatible with canonical mechanisms of crawling-based wound healing and raising the possibility that novel mechanisms may be driving closure. By labeling injured animals with an actin dye, we found that *H. miamia* epidermal cells extend long, actin-rich

cytoplasmic protrusions across the wound edge until they reach the nearest epithelial layer and establish cell-cell contact. This process is dependent on muscle contraction; when animals are anesthetized and immobile, they are unable to form these cellular bridges, and epidermal cells cannot migrate independently. At injury sites that lack underlying muscle connecting the wound edge, wounds heal through the formation of organism-wide contractile purse strings. Together, this work identifies mechanisms by which multiple tissue types work together to close large wounds *in vivo*, indicating a deep conservation of proximate epithelial-mesenchymal interactions in morphogenetic processes.

RESULTS

Epidermal cells in *H. miamia* have an atypical morphology

The acoel *Hofstenia miamia* is an early-diverging marine invertebrate that has emerged as a new research organism for regenerative biology due to its ability to undergo whole-body regeneration and its amenability to mechanistic study[1,2] (Figure 1A-B). *H. miamia* can recover from virtually any injury throughout its lifespan, scarlessly healing wounds and rebuilding lost tissues. Wound healing in epithelial tissues has been studied extensively in traditional model systems, identifying three major and often overlapping modes of wound closure: actomyosin 'purse string' formation, protrusion-based cell crawling, and contraction of underlying cells[3] (Figure 1C). The relative contribution of each cellular process varies significantly between wounding conditions, with factors such as wound size, geometry, tissue type, extracellular matrix composition, and life stage of the animal all influencing the mechanism of closure[3–9]. Most epithelia contain cells sitting atop a basement membrane, an organized layer of extracellular matrix that acts as both an adhesive substrate for the cells and as a physical barrier between epithelia and underlying mesenchymal cells[10–12]. Large injuries typically involve damage to the basement membrane, leading to either wound closure through the formation of actomyosin purse strings, which do not require an intact substrate, and/or the deposition of a transient matrix that provides a substrate for epithelial cell crawling[4,13–16]. These large injuries also require coordination between layers of cells, often relying on contraction of mesenchymal cells underneath the epithelium to drive closure[17–19]. These morphogenetic mechanisms of re-epithelialization are highly evolutionarily conserved and are found in clades across the animal tree of life[13,14,20–22]. The epidermis of *H. miamia*, however, possesses atypical structural characteristics that led us to inquire whether new cellular processes could be at play in this species.

Apart from a basic morphological description and the identification of cell type-specific genes[23–26], the epidermis of *H. miamia* has not been studied in depth. The apical side of *H. miamia* epidermal cells resembles epithelia in other systems, with the cells organized in a polygonal pattern on the surface of the animal (Figure 1D). The basal side of the epidermis, however, differs from typical columnar epithelial cells in two significant ways. First, these cells possess cytoplasmic protrusions that extend into the body of the worm (Figure 1E). These protrusions can be visualized through both transgenic labeling (*EpiA:RFP* animals with mosaic labeling of epidermal cells[25]) and the use of actin dyes (Figure 1E-F). Although the

64 protrusions are irregularly spaced and heterogeneous in number between cells, they generally range from
65 20-35um in length. Second, *H. miamia* lacks a visible basement membrane, and electron-dense
66 structures have not been observed through electron microscopy in any acoel[27]. Instead of resting atop a
67 basement membrane, the basal protrusions end in close proximity to underlying muscle and other
68 mesenchymal tissues[25,27] (Figure 1G). It is unclear whether cell-cell junctions form at the tips of these
69 projections or whether they adhere to an atypical substrate, but there appears to be very little space
70 between cells and these thin protrusions form a dense network of membranes within the animal.
71
72 **Wound closure is driven by the formation of long cellular protrusions that extend over the wound**
73 **edge and connect epithelial tissues**
74 Wound closure is a key aspect of successful regeneration given that it is often the first morphogenetic
75 event that precedes other cellular events. Notably, despite heavy investment in studying whole-body
76 regeneration in many invertebrate systems, the precise cellular mechanisms through which these
77 organisms heal their wounds are not well-studied. Because basement membranes are a conserved
78 element of epithelia, all established models of *in vivo* wound closure (e.g., mouse, zebrafish, fly,
79 nematode, jellyfish) rely on them as key mechanistic components in the healing process[10,28] The atypical
80 morphology of *H. miamia* epidermal cells and lack of basement membrane therefore prompted us to ask
81 how these tissues were able to close after injury. Prior work has revealed that wounds typically heal
82 within the first 24 hours post-amputation (hpa)[1,2]; therefore, to visualize the process of re-epithelialization,
83 we amputated juvenile worms sagittally and stained fragments at intermediate time points with the
84 cytoskeletal dye SiR-actin. Sagittal amputations cut the animal in half, resulting in open epidermal edges
85 around the body as well as through the pharyngeal epithelium (Figure 2A). After amputation, epidermal
86 cells at the periphery formed long extensions across the wound edge, stretching to make contact with the
87 pharyngeal epithelium (Figure 2B-D). We confirmed that these cells were epidermal in nature by use of
88 the *EpiA:RFP* transgenic line; after amputation, labeled cells in the outer epidermis and the pharyngeal
89 epithelium formed protrusions and connected across the wound edge (Supplementary Figure 1A-B).
90 These protrusions appeared in transverse amputations as well, suggesting a shared cellular mechanism
91 across injury orientations (Supplementary Figure 1C). Notably, we did not observe lamellipodia or purse

92 strings, indicating that wound closure in *H. miamia* occurs via processes distinct from those reported in
93 currently studied systems. Amputating the animals in the sagittal plane both maximized the wound edge
94 surface area and allowed for the most reproducible imaging, thus we chose this amputation for all follow-
95 up experiments.

96 Sagittal amputations in *H. miamia* heal through a two-step process: the outer epidermis first
97 connects to the pharyngeal epithelium to close off the open wound (primary closure), then the animal
98 rounds itself up to re-form its cylindrical shape (secondary closure) (Figure 2E, Supplementary Figure
99 1D). Epidermal cells showed signs of actin polarization within the first 3 hours post-amputation (hpa), with
100 small protrusions (~5-20 um) appearing in the outer epidermis oriented towards the wound edge (Figure
101 2B, 2D). Long extensions (~50-80 um) began appearing around 6 hpa, forming more robustly by 10 hpa
102 and connecting to the pharyngeal epithelium (Figure 2C, 2D). These protrusions were primarily detectable
103 in the outer epidermis, but some extensions also originated from pharyngeal epithelial cells (Figure 2D,
104 Supplementary Figure 1E). After the initial bridges formed, neighboring epithelial cells closed the wound
105 through what is likely collective migration. The primary closure takes approximately 30 hours, closing the
106 wound in the anterior half of the animal, and the secondary closure seems to occur as the posterior half of
107 the animal is closing, up to 50 hours post-amputation (Figure 2E, Supplementary Figure 1D).

108 Although less commonly seen than lamellipodia, filopodia have been observed in wound closure
109 in other systems[3,13,29]; however, these protrusions are small and only able to extend across the wound
110 edge after a significant reduction in the wound size. The length of the bridges we observed in *H. miamia*
111 is more similar to those of cytonemes, long protrusions that function as mediators of long-range
112 signaling[30,31]. We do not yet know whether *H. miamia* epidermal bridges play a role in cell signaling, but
113 their structural importance in wound closure suggests that these bridges are likely distinct from
114 cytonemes. To the best of our knowledge, the formation of epithelial bridges seen in *H. miamia* appears
115 to be a unique mode of wound closure. We therefore sought to understand the molecular mechanisms
116 driving this phenomenon.

117

118 **Despite an atypical cellular presentation, wound closure in *H. miamia* requires conserved**
119 **actomyosin pathways**

120 To investigate the mechanisms behind these epithelial bridges, we first turned to conserved pathways of
121 actomyosin contractility. Wound closure through cell crawling is facilitated through the formation of actin-
122 based membrane protrusions (such as lamellipodia or filopodia) in cells at the periphery of a wound that
123 drive migration into the gap[9,32,33]. Actomyosin contractility is essential in this crawling mechanism for both
124 retraction at the rear of migrating cells and in the formation of tension between adhesion points[6,13,34].
125 Purse string closure is similarly driven by actin contractility; cells around the wound form a supracellular
126 cable, contracting and bringing the edges of cells inwards to pinch off the gap[32,35,36]. Both mechanisms
127 require dynamic actin and enable the edges of existing cells to meet across the open wound, restoring
128 the integrity of the epithelial sheet through the reestablishment of cell junctions[9]. Although wound closure
129 in *H. miamia* doesn't present as typical lamellipodia or purse strings, we asked whether the same
130 underlying molecular pathways were being used.

131 The SiR-actin dye labeling showed an anisotropic enrichment of actin towards the wound edge,
132 implicating actin dynamics in the formation of these extensions (Figure 2). We therefore used
133 phamacological inhibition to assess the role of actomyosin contractility in *H. miamia* wound closure
134 (Figure 2A). We first identified the complement of cytoskeletal components encoded in the *H. miamia*
135 genome (see Methods). *H. miamia* expresses putative homologs of all major components associated with
136 cell contractility (e.g., myosin), adhesion (e.g., cadherins, integrins), and general cytoskeletal activity (e.g.,
137 actin, Rho family GTPases), suggesting that conserved molecular pathways might be driving different
138 cellular behaviors (Supplementary File 1).

139 To test the role of these cytoskeletal pathways, we first treated the animals with the inhibitor
140 cytochalasin D to block actin polymerization[6,37]. As anticipated, cytochalasin D treatment prevented
141 wound closure, with animals unable to form any epidermal protrusions between 0-30 hours (Figure 3B-C).
142 The small GTPase Rho drives cell contractility through signaling to the downstream proteins Rho kinase
143 (ROCK) and myosin light chain (MLC), leading to the accumulation and contraction of actin and myosin at
144 cell membranes[29]. To perturb this pathway, we treated animals with the small molecule compounds Y-
145 27632 (which inhibits ROCK) and blebbistatin (which inhibits MLC). Animals treated with both inhibitors
146 showed a significant reduction in wound closure at 30 hpa (Figure 3B-C). Epidermal cells in blebbistatin-
147 treated animals extended short protrusions, but they were unable to bridge the gap and merge the two

148 epithelial sheets to properly heal (Figure 3D). These data demonstrate that the Rho/ROCK/MLC pathway
149 of actomyosin contractility is still required for wound closure, even in the absence of canonical cellular
150 phenotypes.
151
152 **Wound closure through epidermal protrusions is dependent on proximate muscle contraction**
153 Despite the functional importance of conserved contractility pathways across the whole animal, the
154 epidermal protrusions we observed in *H. miamia* didn't appear to be forming purse string-based
155 structures during wound closure. This suggested that the contractile force driving closure might involve
156 cell layers other than the epidermis. Contraction of proximate muscle is an essential component of wound
157 closure in both vertebrates and invertebrates[15,18,38,39], and we therefore asked whether muscle contraction
158 was similarly involved in wound closure in *H. miamia*. *H. miamia* have an extensive network of muscle
159 throughout their bodies, comprising four broad populations: peripheral muscle, body wall muscle,
160 parenchymal muscle, and pharynx muscle (Figure 4A)[25]. Immediately after both sagittal and transverse
161 amputation, we stained fragments with an antibody recognizing tropomyosin[40] and noted the presence of
162 underlying parenchymal muscle between the outer epidermis and the pharyngeal epithelium prior to any
163 wound closure. This muscle was orientated in the same direction as the bridges we observed during
164 epithelial wound closure (Figure 4B, Supplementary Figure 1C, Supplementary Figure 2A), leading us to
165 hypothesize that contraction of these parenchymal muscle fibers might facilitate the formation or
166 maintenance of these extensions (Figure 4C). We performed live imaging of amputated animals and saw
167 that fragments undergo substantial, repeated muscle contraction immediately after injury, then continue
168 contracting throughout the process of wound closure. As hypothesized, the major plane of contraction
169 mirrors the directionality of wound closure after sagittal amputation (Video 1). We observed the same
170 trend when animals were transversely amputated; muscle contraction appeared to be bringing the outer
171 epidermis in closer proximity to the pharyngeal epithelium (Video 1). To test the functional role of muscle
172 contraction, we anesthetized animals in 0.1% tricaine, which slows muscle contraction (Video 2). In the
173 presence of tricaine, wound closure is completely blocked (Figure 4D-E). Despite the failure of wound
174 closure, epidermal cells formed ample filopodia - indicating that actin is able to become polarized within
175 the epidermis, but that bridges cannot form without muscle contraction (Figure 4F).

176 The lack of wound closure could be explained by several potential mechanisms that are not
177 mutually exclusive and have all been observed in other systems: (1) muscle contraction is directly
178 bringing the wound edges together, serving as the driving force behind re-epithelialization[38], (2) muscle
179 contraction is stimulating remodeling of the ECM, either by triggering release of matrix remodelers or by
180 reorienting ECM proteins themselves[17], or (3) muscle contraction is triggering essential signaling
181 pathways through mechanotransduction[41]. It takes at least 6 hours for bridges to form, suggesting that
182 there is likely a series of cellular events occurring in the first 6-10 hours post amputation that enable the
183 initiation of wound closure. To determine if there is a temporal role for muscle contraction, we performed
184 treatments with tricaine at different time windows during healing. Animals were either: 1) treated with
185 tricaine for 10 hours following amputation, then placed into fresh sea water for 20 hours, or 2) kept in sea
186 water for 10 hours, then treated with tricaine for 20 hours (Supplementary Figure 2B). Animals kept in
187 tricaine for the first 10 hours recovered and were able to close their wounds at comparable rates to
188 control animals. In contrast, animals placed in tricaine after the first 10 hours were unable to undergo
189 wound closure, similar to animals kept in tricaine for all 30 hours (Supplementary Figure 2C-D).
190 Mechanotransduction and ECM remodeling cannot be ruled out at this time, but these data suggest that
191 muscle contraction is functioning primarily as a physical driver of wound closure, helping bridge the gap
192 between epithelial sheets.
193 To confirm the importance of underlying muscle orientation in wound closure, we asked what
194 might occur after an injury that forced the fragment to contract in a different direction. We reasoned that
195 cutting animals transversely below the pharynx would remove the pharyngeal muscle and parenchymal
196 muscle that connects the pharynx and outer epidermis, leaving behind primarily peripheral muscle and
197 body wall muscle and likely altering the ability of muscle contraction to directly bring the wound edges
198 together (Figure 4G). Indeed, the injured epidermis in animals cut in this manner did not form epidermal
199 bridges; instead, wounds gradually closed via the formation of purse string-like structures (Figure 4H-I).
200 Peripheral and body wall muscle underlying the epidermis was brought closer together during this
201 process of wound closure but was never seen bridging the wound edges together, suggesting a switch in
202 closure mechanism (Figure 4H). Together, these data demonstrate a mechanism by which proximate
203 tissue interactions drive large-scale wound healing in a regenerative invertebrate.

DISCUSSION

Here, we examined the mechanism of wound closure in the acoel *Hofstenia miamia* and found a new cellular mechanism in which epithelial cells extend long, finger-like protrusions across a large wound gap that allow the animal to 'suture' itself back together prior to whole-body regeneration. Despite lacking cellular and morphological similarities to previously reported processes of wound closure, this process is dependent on conserved molecular pathways of cytoskeletal dynamics and cell contractility. Analogous to the process of mammalian wound healing, the mechanical force driving these epidermal extensions comes from contraction of underlying muscle[3,38,42]. Without muscle contraction, epidermal cells polarize their actin cytoskeletons and form filopodia, but they cannot breach the wound gap to re-epithelialize. Previous work on wound closure has focused on a handful of model systems, and our work highlights the power of broadened taxonomic sampling to identify new biological mechanisms.

Although the mechanism of wound closure in *H. miamia* appears morphologically distinct from wound healing in other species, it shares similarities with other morphogenetic processes that require the fusion of epithelial sheets. Thorax closure during *Drosophila melanogaster* development is dependent on contraction of the underlying epidermal layer, although this contraction is driven by the delamination and apoptosis of epidermal cells rather than muscle contraction[43]. The extension of filopodial protrusions as a mechanism of connecting epithelial sheets has been observed in systems such as *D. melanogaster* dorsal closure[44,45] and cardiogenesis[46], as well as mammalian lens morphogenesis[47], neurogenesis[48], and neural tube closure[49]. Future work establishing *H. miamia* as a model system for cell biology will shed light on how evolutionarily conserved mechanisms could drive morphogenetic processes in repair and regeneration.

REFERENCES

1. Srivastava, M., Mazza-Curll, K. L., van Wolfswinkel, J. C. & Reddien, P. W. Whole-Body Acoel Regeneration Is Controlled by Wnt and Bmp-Admp Signaling. *Curr. Biol.* **24**, 1107–1113 (2014).
2. Raz, A. A., Srivastava, M., Salvamoser, R. & Reddien, P. W. Acoel regeneration mechanisms indicate an ancient role for muscle in regenerative patterning. *Nat. Commun.* **8**, 1260 (2017).
3. Begnaud, S., Chen, T., Delacour, D., Mège, R.-M. & Ladoux, B. Mechanics of epithelial tissues during gap closure. *Curr. Opin. Cell Biol.* **42**, 52–62 (2016).
4. Ehrlich, H. P. Wound closure: evidence of cooperation between fibroblasts and collagen matrix. *Eye* **2**, 149–157 (1988).
5. Basan, M., Elgeti, J., Hannezo, E., Rappel, W.-J. & Levine, H. Alignment of cellular motility forces with tissue flow as a mechanism for efficient wound healing. *Proc. Natl. Acad. Sci.* **110**, 2452–2459 (2013).
6. Henson, J. H. *et al.* Wound Closure in the Lamellipodia of Single Cells: Mediation by Actin Polymerization in the Absence of an Actomyosin Purse String. *Mol. Biol. Cell* **13**, 1001–1014 (2002).
7. Vedula, S. R. K. *et al.* Mechanics of epithelial closure over non-adherent environments. *Nat. Commun.* **6**, 6111 (2015).
8. Xu, H. *et al.* Geometry-mediated bridging drives nonadhesive stripe wound healing. *Proc. Natl. Acad. Sci.* **120**, e2221040120 (2023).
9. Lim, S. E., Vicente-Munuera, P. & Mao, Y. Forced back into shape: Mechanics of epithelial wound repair. *Curr. Opin. Cell Biol.* **87**, 102324 (2024).
10. Fidler, A. L. *et al.* Collagen IV and basement membrane at the evolutionary dawn of metazoan tissues. *eLife* **6**, e24176 (2017).
11. Pastor-Pareja, J. C. Atypical basement membranes and basement membrane diversity – what is normal anyway? *J. Cell Sci.* **133**, jcs241794 (2020).
12. Cote, L. E. & Feldman, J. L. Won’t You be My Neighbor: How Epithelial Cells Connect Together to Build Global Tissue Polarity. *Front. Cell Dev. Biol.* **10**, 887107 (2022).

13. Kamran, Z. *et al.* In vivo imaging of epithelial wound healing in the cnidarian Clytia hemisphaerica demonstrates early evolution of purse string and cell crawling closure mechanisms. *BMC Dev. Biol.* **17**, 17 (2017).

14. Huang, T. *et al.* Re-epithelialization of large wound in paedomorphic and metamorphic axolotls. *J. Morphol.* **278**, 228–235 (2017).

15. Shaw, T. J., Osborne, M., Ponte, G., Fiorito, G. & Andrews, P. L. R. Mechanisms of wound closure following acute arm injury in Octopus vulgaris. *Zool. Lett.* **2**, 8 (2016).

16. Chakraborty, S. *et al.* Agrin-Matrix Metalloproteinase-12 axis confers a mechanically competent microenvironment in skin wound healing. *Nat. Commun.* **12**, 6349 (2021).

17. Brauer, E. *et al.* Collagen Fibrils Mechanically Contribute to Tissue Contraction in an In Vitro Wound Healing Scenario. *Adv. Sci.* **6**, 1801780 (2019).

18. Valero, C., Javierre, E., García-Aznar, J. M. & Gómez-Benito, M. J. A Cell-Regulatory Mechanism Involving Feedback between Contraction and Tissue Formation Guides Wound Healing Progression. *PLoS ONE* **9**, e92774 (2014).

19. Yannas, I. V. & Tzeranis, D. S. Mammals fail to regenerate organs when wound contraction drives scar formation. *Npj Regen. Med.* **6**, 39 (2021).

20. Doerr, S., Zhou, P. & Ragkousi, K. Origin and development of primary animal epithelia. *BioEssays* **46**, 2300150 (2024).

21. Gumbrys, A. Epidermis and Re-epithelialization in *Schmidtea mediterranea*. (2017) doi:10.21954/OU.RO.0000C71C.

22. Lavrov, A. I., Bolshakov, F. V., Tokina, D. B. & Ereskovsky, A. V. Sewing up the wounds : The epithelial morphogenesis as a central mechanism of calcaronean sponge regeneration. *J. Exp. Zoolog. B Mol. Dev. Evol.* **330**, 351–371 (2018).

23. Kimura, J. O., Ricci, L. & Srivastava, M. Embryonic development in the acoel *Hofstenia miamia*. *Development* **148**, dev188656 (2021).

24. Bump, P., Loubet-Senear, K., Arnold, S. & Srivastava, M. Chromatin profiling data indicate regulatory mechanisms for differentiation during development in the acoel *Hofstenia miamia*. Preprint at https://doi.org/10.1101/2023.12.05.570175 (2023).

280 25. Ricci, L. & Srivastava, M. Transgenesis in the acoel worm Hofstenia miamia. *Dev. Cell* **56**, 3160-
281 3170.e4 (2021).
282 26. Hulett, R. E. *et al.* Acoel single-cell atlas reveals expression dynamics and heterogeneity of adult
283 pluripotent stem cells. *Nat. Commun.* **14**, 2612 (2023).
284 27. Dorey, A. E. The organization and replacement of the epidermis in acoelous turbellarians. *J. Cell*
285 *Sci.* **S3-106**, 147–172 (1965).
286 28. Sakar, M. S. *et al.* Cellular forces and matrix assembly coordinate fibrous tissue repair. *Nat.*
287 *Commun.* **7**, 11036 (2016).
288 29. Ramon-Mateu, J., Ellison, S. T., Angelini, T. E. & Martindale, M. Q. Regeneration in the
289 ctenophore Mnemiopsis leidyi occurs in the absence of a blastema, requires cell division, and is
290 temporally separable from wound healing. *BMC Biol.* **17**, 80 (2019).
291 30. Daly, C. A., Hall, E. T. & Ogden, S. K. Regulatory mechanisms of cytoneme-based morphogen
292 transport. *Cell. Mol. Life Sci.* **79**, 119 (2022).
293 31. Ruhoff, V. T., Leijnse, N., Doostmohammadi, A. & Bendix, P. M. Filopodia: integrating cellular
294 functions with theoretical models. *Trends Cell Biol.* S0962892424001132 (2024)
295 doi:10.1016/j.tcb.2024.05.005.
296 32. Bement, W. M., Mandato, C. A. & Kirsch, M. N. Wound-induced assembly and closure of an
297 actomyosin purse string in Xenopus oocytes. *Curr. Biol.* **9**, 579–587 (1999).
298 33. Nobes, C. D. & Hall, A. Rho, Rac, and Cdc42 GTPases regulate the assembly of multimolecular
299 focal complexes associated with actin stress fibers, lamellipodia, and filopodia. *Cell* **81**, 53–62 (1995).
300 34. Tang, V. W. Cell–cell adhesion interface: orthogonal and parallel forces from contraction,
301 protrusion, and retraction. *F1000Research* **7**, 1544 (2018).
302 35. Da Costa, A. D. S. *et al.* Fibroblasts Close a Void in Free Space by a Purse-String Mechanism.
303 *ACS Appl. Mater. Interfaces* **14**, 40522–40534 (2022).
304 36. Rodriguez-Diaz, A. *et al.* Actomyosin purse strings: Renewable resources that make
305 morphogenesis robust and resilient. *HFSP J.* **2**, 220–237 (2008).

306 37. Donaldson, D. J. & Dunlap, M. K. Epidermal cell migration during attempted closure of skin
307 wounds in the adult newt: Observations based on cytochalasin treatment and scanning electron
308 microscopy. *J. Exp. Zool.* **217**, 33–43 (1981).
309 38. Li, B. & Wang, J. H.-C. Fibroblasts and myofibroblasts in wound healing: Force generation and
310 measurement. *J. Tissue Viability* **20**, 108–120 (2011).
311 39. Chandebois, R. THE DYNAMICS OF WOUND CLOSURE AND ITS ROLE IN THE
312 PROGRAMMING OF PLANARIAN REGENERATION. II - DISTALIZATION. *Dev. Growth Differ.* **22**,
313 693–704 (1980).
314 40. Hulett, R. E., Potter, D. & Srivastava, M. Neural architecture and regeneration in the acoel
315 *Hofstenia miamia*. *Proc. R. Soc. B Biol. Sci.* **287**, 20201198 (2020).
316 41. Martino, F., Perestrelo, A. R., Vinarský, V., Pagliari, S. & Forte, G. Cellular Mechanotransduction:
317 From Tension to Function. *Front. Physiol.* **9**, 824 (2018).
318 42. Fenteany, G., Janmey, P. A. & Stossel, T. P. Signaling pathways and cell mechanics involved in
319 wound closure by epithelial cell sheets. *Curr. Biol.* **10**, 831–838 (2000).
320 43. Athilingam, T. *et al.* Proximate larval epidermal cell layer generates forces for Pupal thorax
321 closure in *Drosophila*. *Genetics* **221**, iyac030 (2022).
322 44. Martín-Blanco, E., Pastor-Pareja, J. C. & García-Bellido, A. JNK and *decapentaplegic* signaling
323 control adhesiveness and cytoskeleton dynamics during thorax closure in *Drosophila*. *Proc. Natl. Acad.*
324 *Sci.* **97**, 7888–7893 (2000).
325 45. Jacinto, A. *et al.* Dynamic actin-based epithelial adhesion and cell matching during Drosophila
326 dorsal closure. *Curr. Biol.* **10**, 1420–1426 (2000).
327 46. Zhang, S., Amourda, C., Garfield, D. & Saunders, T. E. Selective Filopodia Adhesion Ensures
328 Robust Cell Matching in the Drosophila Heart. *Dev. Cell* **46**, 189-203.e4 (2018).
329 47. Chauhan, B. K. *et al.* Cdc42- and IRSp53-dependent contractile filopodia tether presumptive lens
330 and retina to coordinate epithelial invagination. *Development* **136**, 3657–3667 (2009).
331 48. Kasioulis, I. *et al.* A lateral protrusion latticework connects neuroepithelial cells and is regulated
332 during neurogenesis. *J. Cell Sci.* jcs.259897 (2022) doi:10.1242/jcs.259897.

333 49. Pyrgaki, C., Trainor, P., Hadjantonakis, A.-K. & Niswander, L. Dynamic imaging of mammalian
334 neural tube closure. *Dev. Biol.* **344**, 941–947 (2010).
335

336 **MATERIALS AND METHODS**

337 ***H. miamia* strains and husbandry**

338 Adult worms were housed in artificial sea water (ASW) (37 ppt, pH 7.70-8.00) in plastic boxes within 21°C
339 incubators. Embryos were collected from adult boxes and placed into petri dishes for development. Once
340 hatched, juvenile worms were transferred to tanks for post-embryonic growth. All animals were fed twice a
341 week; adult worms were fed brine shrimp (Artemia, Brine Shrimp Direct) and juvenile hatchlings were fed
342 rotifers (*Brachionus plicatilis*, Reed Mariculture). *EpiA:RFP* worms were generated as previously
343 described[25].

344

345 **Amputations and sample preparation**

346 Juvenile worms were isolated and starved for 1-2 weeks prior to use to minimize autofluorescence of
347 ingested food. For regeneration experiments, animals were placed in 1mg/mL ethyl 3-aminobenzoate,
348 methanesulfonic acid ("tricaine", stock solution 5mg/mL of ASW) (Thermo Fisher, AC118000100) in ASW
349 in a petri dish for 3-5 minutes until they stopped swimming, then amputated using a scalpel. After
350 amputation, fragments were transferred to a dish containing fresh ASW until their designated time point.
351 For fixation, animals were placed in 4% paraformaldehyde (PFA) (Thomas Scientific, C993M31) in ASW
352 for 1 hour at room temperature. The PFA was removed and animals were washed with PBST (PBS +
353 0.1% Triton-X-100) three times prior to staining for immunofluorescence staining. For transverse cuts,
354 animals were cut once transversely and transferred to fresh ASW until their designated time point.
355 Animals were cut transversely once again, right above the previous cut. These fragments were then
356 immediately fixed in 4% PFA in ASW as described previously.

357

358 **Small molecule inhibitors and treatment with anesthetics**

359 For small molecule inhibitor experiments, animals were first amputated as described above, then flushed
360 with ASW to remove tricaine prior to incubation in designated inhibitors. Animals were left in inhibitor for
361 10-30 hours, depending on the experiment. Cytochalasin D (Sigma-Aldrich, C8273) and blebbistatin
362 (Sigma-Aldrich, B0560) were dissolved in DMSO per manufacturer instructions, then diluted in ASW for
363 use at 1μg/mL and 25μM, respectively. Y-27632 (Stem Cell Technologies, 72307) was dissolved in water

364 per manufacturer instructions, then diluted in ASW for use at 10μM. For tricaine time point experiments,
365 animals were left in 0.5mg/mL tricaine for 10-30 hours.
366
367 **Immunostaining**
368 For antibody staining, all steps were carried out using an orbital shaker. Fixed animals were washed in
369 PBST for 3x5 minutes, then placed in blocking solution (PBST + 10% goat serum (Thermo Fisher,
370 16210072)) for one hour at room temperature. Animals were then placed in primary antibody in block
371 solution for two nights at 4°C. Primary antibody was washed out with PBST, 6x20 minutes. Animals were
372 then blocked once again for one hour at room temperature, then incubated with secondary antibody
373 (1:800) (Thermo Fisher, A-11011) in blocking solution overnight at 4°C. The next day, secondary antibody
374 was washed out using PBST, 6x20 minutes. Finally, animals were incubated in PBST with Hoechst
375 (1:500) (Invitrogen, H3570) and SiR-actin (1:1000) (Cytoskeleton, CY-SC001) for 90 minutes at room
376 temperature prior to mounting. All samples were mounted on double cover slips using Prolong Glass
377 Antifade Mountant (Thermo Fisher, P36980). If animals were only stained with SiR-actin, they were
378 placed in SiR-actin and Hoechst in PBST for 90 minutes at room temperature, then mounted immediately.
379 The custom *H. miamia* Tropomyosin anitbody[40] (Rabbit IgG) was used at 1μg/mL.
380
381 **Microscopy and image processing**
382 All images were collected using 10x/0.25x (dry), 20x/0.75x (dry), or 63x/1.40 (oil) fluorescent objectives
383 on a Leica DMI SP8 inverted confocal microscope, equipped with Leica Application Suite software.
384
385 **Quantification of wound closure**
386 To quantify wound closure after sagittal cuts, images of SiR-actin-stained fragments were imported into
387 FIJI. Because of mounting imperfections, only one side of each animal was measured, choosing the side
388 with the clearest signal for the most accurate quantification. 6-12 animals were quantified per time point
389 and condition. Within FIJI, the Measure function was used to quantify: 1) the length of the pharynx and 2)
390 the cumulative distance of connected tissue between the epidermis and the pharyngeal epithelium. The
391 percentage of wound closure was determined by dividing the closed distance by the total pharynx length.

392 For quantification of wound closure in transverse cuts, images were taken of both the wound edge and
393 the open edge of each sample, using FIJI to measure the open area of each side. The percentage of
394 wound closure was determined by dividing the open area of the wound edge by the total open area, then
395 subtracting that from 1.
396
397 **Statistical analyses**
398 Data with two or more factors were analyzed using two-way ANOVA with Dunnett's multiple comparisons
399 test. Data comparing changes in one condition over different time points were analyzed by one-way
400 ANOVA with Dunnett's multiple comparisons test. A two-tailed unpaired *t*-test with Welch's correction was
401 used to compare data between two independent groups. All statistical tests are stated in figure legends. *P*
402 values were obtained using GraphPad PRISM and used to determine the level of varying significance
403 between experimental groups; groups were considered different when $P<0.05$.
404
405 **Gene identification and phylogenetic analysis**
406 To identify putative homologs of contractility-associated genes, we used BLAST to query known genes
407 from *D. rerio, D. melanogaster, H. vulgaris,* or *N. vectensis* against the *H. miamia* transcriptome[26]. Protein
408 sequences were obtained from GenBank, and accession numbers are provided in Supplementary File 1.
409 Genes were considered putative homologs based on a combination of sequence similarity, E Value, and
410 reverse BLAST hits.

ACKNOWLEDGEMENTS

APK is a Fellow of the Jane Coffin Childs Memorial Fund for Medical Research. This project was supported by grants from the National Institute of General Medical Sciences of the NIH to MS: R35GM128817 and R35GM153252. Many thanks to members of the Srivastava Lab for feedback on the manuscript.

AUTHOR CONTRIBUTIONS

Conceptualization: A.P.K. and M.S., Data curation: A.P.K., Formal analysis: A.P.K., Funding acquisition: A.P.K. and M.S., Investigation: A.P.K., Methodology: A.P.K. and M.S., Project administration: A.P.K. and M.S., Resources: M.S., Supervision: M.S., Validation: A.P.K., Visualization: A.P.K., Writing – original draft: A.P.K., Writing – review & editing: A.P.K. and M.S.

COMPETING INTERESTS

None declared.

425 **FIGURES AND FIGURE LEGENDS**

426 **Figure 1. *Hofstenia miamia* epidermal cells have an atypical morphology.**

427 (A) A juvenile *Hofstenia miamia.* (B) A simplified phylogenetic tree showing the position of *Hofstenia*
428 *miamia* (red, Xenoacoelomorpha) relative to other clades as the likely sister group to bilaterians (solid
429 line) or sister to Ambulacraria (dotted line). mya = million years ago. (C) Schematics of the three main
430 mechanisms involved in wound closure: purse string formation (top), lamellipodia crawling (middle), and
431 the combination of cell crawling with contraction of the proximal layer (bottom). (D) Organization of the *H.*
432 *miamia* epidermis, showing polygonal organization at the apical ends of cells. (E) Morphology of
433 individual epidermal cells, visualized by *EpiA:RFP* transgenic labeling. A: apical, B: basal. (F) Apicobasal
434 lateral view of the epidermis through either *EpiA:RFP* transgenic labeling (top) or staining with SiR-actin
435 (bottom). (G) Confocal images showing the proximity of muscle (visualized through immunofluorescence
436 staining for tropomyosin) to the epidermis (labeled with SiR-actin). Scale bars: 50 μm (A), 20μm (D), 5μm
437 (E), 25μm (F-G).

438

439 **Figure 2. Epidermal cells use long cytoplasmic extensions to facilitate wound closure.**

440 (A) Schematic showing orientation of *H. miamia* following sagittal amputation. (B-C) Representative
441 images of wound closure following sagittal amputation at early (B, 0-6hpa) and late (C, 10-50hpa) time
442 points. The outer epidermis is pseudocolored in red and the edge of the pharynx is outlined with a black
443 dashed line for clarity. (D) High-magnification images of epidermal protrusions extending across the
444 wound edge between 3-10hpa. The pharynx is outlined with a black dashed line for clarity. Asterisks
445 indicate protrusions originating from the pharyngeal epithelium. (E) Schematic of wound closure in *H.*
446 *miamia*. Scale bars: 50μm (B-C), 10μm (D). hpa = hours post-amputation.

447

448 **Figure 3. Conserved pathways of actomyosin contractility are essential for re-epithelialization.**

449 (A) Simplified schematic of Rho/ROCK/MLC pathway driving actomyosin contractility and the small
450 molecules used in this figure. (B-C) Representative images (B) and quantification (C) of wound closure in
451 control (DMSO), cytochalasin D, Y-27632, and blebbistatin conditions at 10 and 30hpa. The outer
452 epidermis is pseudocolored in red (DMSO), yellow (cytochalasin D), blue (Y-27632), or green

453 (blebbistatin) the edge of the pharynx is outlined with a dashed line for clarity. (D) High-magnification
454 image showing the presence of cytoplasmic extensions in blebbistatin-treated animals at 30hpa. Data
455 represent n=10 worms per condition and show mean ± s.e.m. Comparisons by two-way ANOVA with
456 Dunnett's multiple comparisons test; ns=not significant. Scale bars: 50μm (B), 10μm (D). hpa = hours
457 post-amputation.
458
459 **Figure 4. Contraction and organization of underlying muscle drives wound closure.**
460 (A) Schematic showing the organization of four main types of muscle in *H. miamia*. (B) Images showing
461 the organization of parenchymal muscle in sagittally- and transversely-cut animals, visualized by
462 immunofluorescence staining for tropomyosin. (C) Schematic showing the correlation between orientation
463 of parenchymal muscle (blue) and the direction of protrusions that drive wound closure (red). (D-E)
464 Representative images (D) and quantification (E) of wound closure in control and tricaine-treated animals
465 at 10 and 30hpa. The outer epidermis is pseudocolored in red (control) or purple (tricaine) and the edge
466 of the pharynx is outlined with a dashed line for clarity. (F) High-magnification image showing the
467 presence of filopodia (red arrowheads) in epidermal cells in the presence of tricaine. (G) Schematic
468 showing the remaining muscle types after transverse amputation below the pharynx. (H-I) Representative
469 images (H) and quantification (I) of wound closure at 3, 6, and 10hpa after transverse amputation below
470 the pharynx. Red asterisk indicates the base of the pharynx, visible in open wounds. Red arrowheads
471 indicate rings of actin density similar to those of traditional purse strings. Data represent n=8-10 worms
472 per time point and show mean ± s.e.m. Comparisons by unpaired t test with Welch's correction (D) or
473 one-way ANOVA with Dunnett's multiple comparisons test (H); ns=not significant. Scale bars: 50μm
474 (B,D,H), 10μm (F). hpa = hours post amputation.

475 **SUPPLEMENTARY FIGURES AND TABLES**

476 **Supplementary Figure 1. Wound closure in *H. miamia* is driven by epidermal cells in both**
477 **transverse and sagittal cuts.**

478 (A-B) *EpiA:RFP* transgenic animals cut sagittally have mosaic expression of RFP in both the epidermis
479 and the pharyngeal epithelium (A), and these cells are part of the SiR-actin-labeled population that is
480 forming protrusions during wound closure (B). (C) Amputation through the transverse plane shows the
481 formation of protrusions between the pharyngeal epithelium and the outer epidermis. (D) Time course of
482 wound closure showing primary (20-30hpa) and secondary (40-50hpa) closure. (E) High-magnification
483 image showing protrusions originating from the pharyngeal epithelium (red asterisks). Scale bars: 50μm
484 (A,C,D), 20μm (B,E). hpa = hours post-amputation.

485

486 **Supplementary Figure 2. Muscle contraction drives wound closure.**

487 (A) Time course of wound closure showing the reorganization of muscle through immunofluorescence for
488 tropomyosin. (B) Schematic of tricaine timing experiment. (C) Representative images showing wound
489 closure in control, tricaine, 10h tricaine (+ 20h ASW), or 10h ASW (+ 20h tricaine) conditions. (D)
490 Quantification of wound closure across tricaine conditions. Data represent n=8 worms per condition and
491 show mean ± s.e.m. Comparisons by one-way ANOVA with Dunnett's multiple comparisons test; ns=not
492 significant. Scale bars: 50um.

493

494 **Supplementary File 1. Putative *Hofstenia miamia* homologs for major components of cell**
495 **contractility, adhesion, and migration.**

496

497 **Supplementary Video 1. The directionality of wound closure mirrors the major plane of**
498 **contraction after amputation.**

499 Video shows animals cut in the sagittal (L) and transverse (R) planes.

500

501 **Supplementary Video 2. Tricaine slows muscle contraction in *H. miamia*.**

502 Animals are anesthetized in 1mg/mL tricaine in ASW.

Figure 1

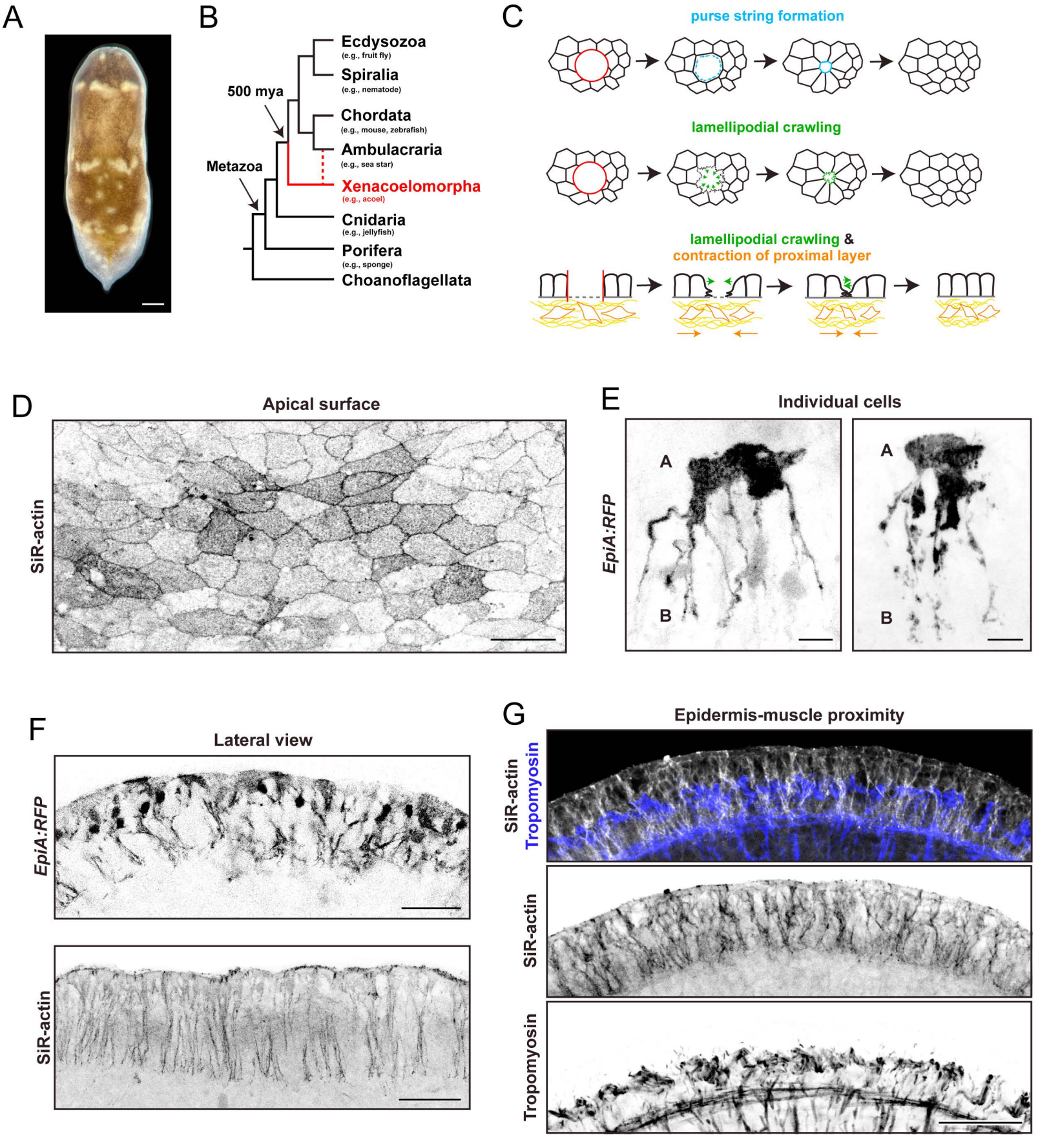
A
B
Ecdysozoa
(e.g., fruit fly)
Spiralia
(e.g., nematode)
500 mya
Chordata
(e.g., mouse, zebrafish)
Ambulacraria
(e.g., sea star)
Metazoa
Xenacoelomorpha
(e.g., acoel)
Cnidaria
(e.g., jellyfish)
Porifera
(e.g., sponge)
Choanoflagellata
C
purse string formation
lamellipodial crawling
lamellipodial crawling &
contraction of proximal layer
D
Apical surface
SiR-actin
E
Individual cells
EpiA:RFP
A
B
A
B
F
Lateral view
EpiA:RFP
SiR-actin
G
Epidermis-muscle proximity
SiR-actin
Tropomyosin
SiR-actin
Tropomyosin

Figure 2

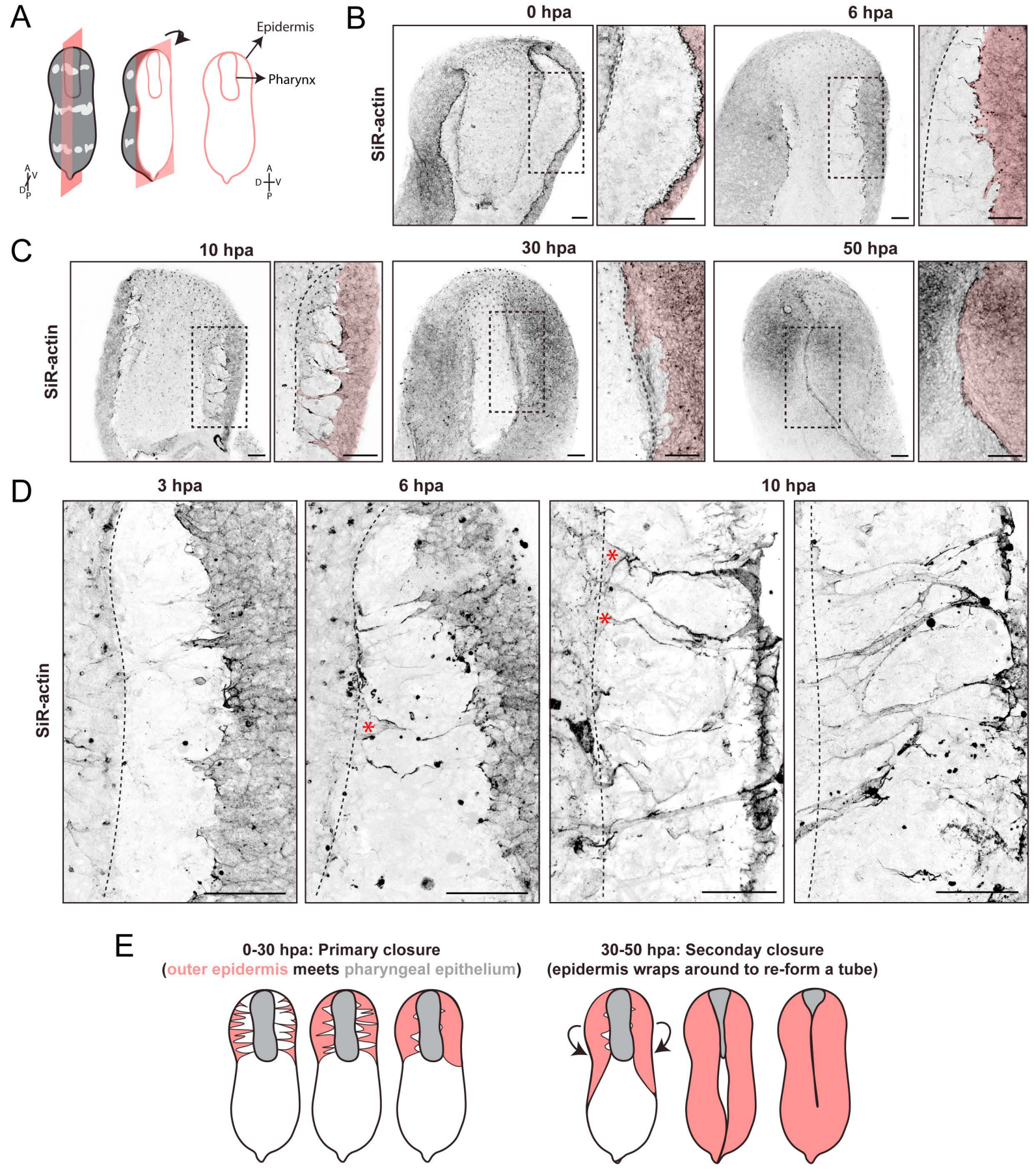
A
Epidermis
Pharynx
A
V
D
P
B
0 hpa
6 hpa
SiR-actin
C
10 hpa
30 hpa
50 hpa
SiR-actin
D
3 hpa
6 hpa
10 hpa
SiR-actin
E
0-30 hpa: Primary closure
(outer epidermis meets pharyngeal epithelium)
30-50 hpa: Seconday closure
(epidermis wraps around to re-form a tube)

Figure 3

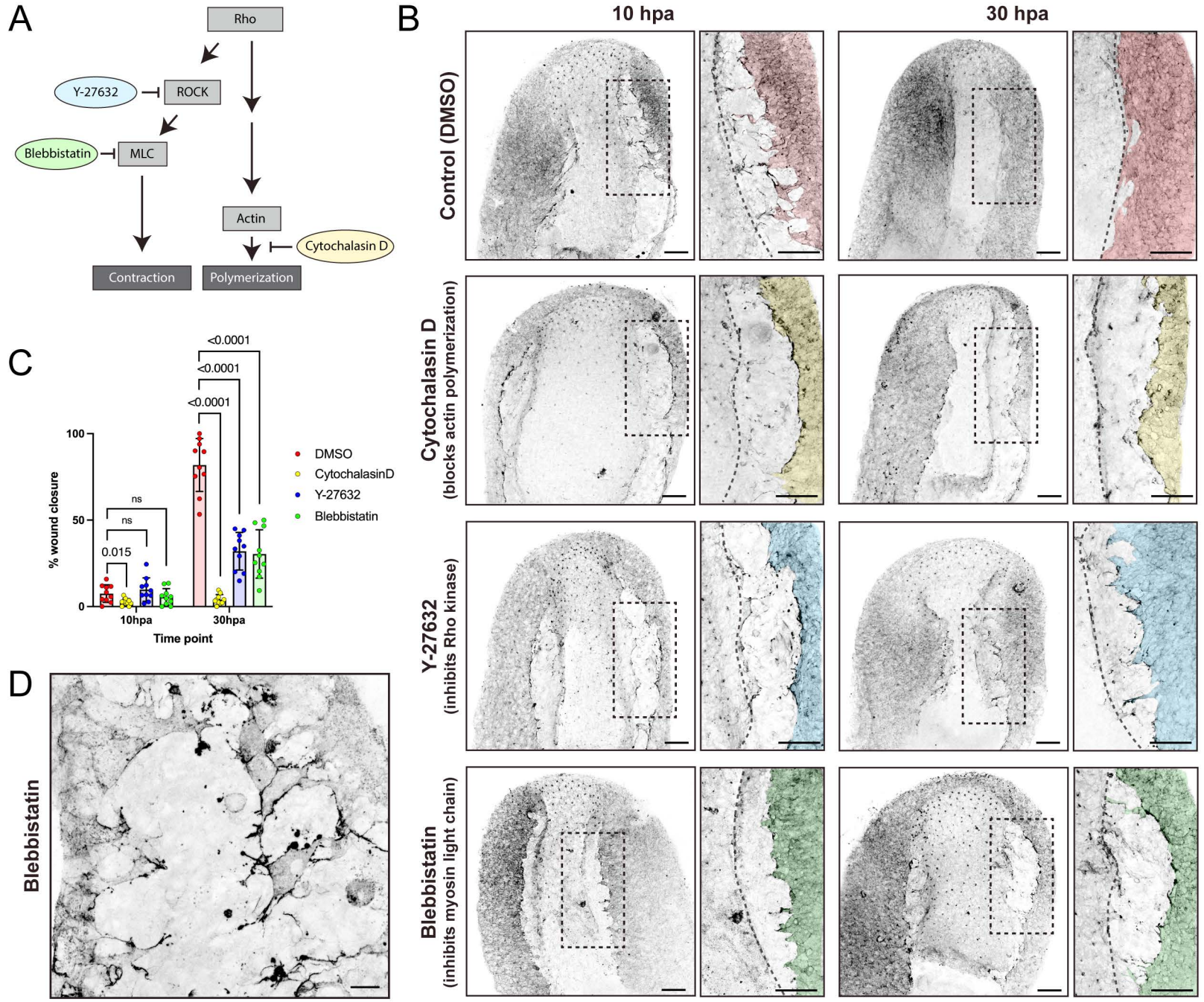
A
Rho
Y-27632
ROCK
Blebbistatin
MLC
Actin
Cytochalasin D
Contraction
Polymerization
B
10 hpa
30 hpa
Control (DMSO)
Cytochalasin D
(blocks actin polymerization)
Y-27632
(inhibits Rho kinase)
Blebbistatin
(inhibits myosin light chain)
C
% wound closure
Time point
10hpa
30hpa
ns
ns
0.015
<0.0001
<0.0001
<0.0001
DMSO
CytochalasinD
Y-27632
Blebbistatin
D
Blebbistatin

Figure 4

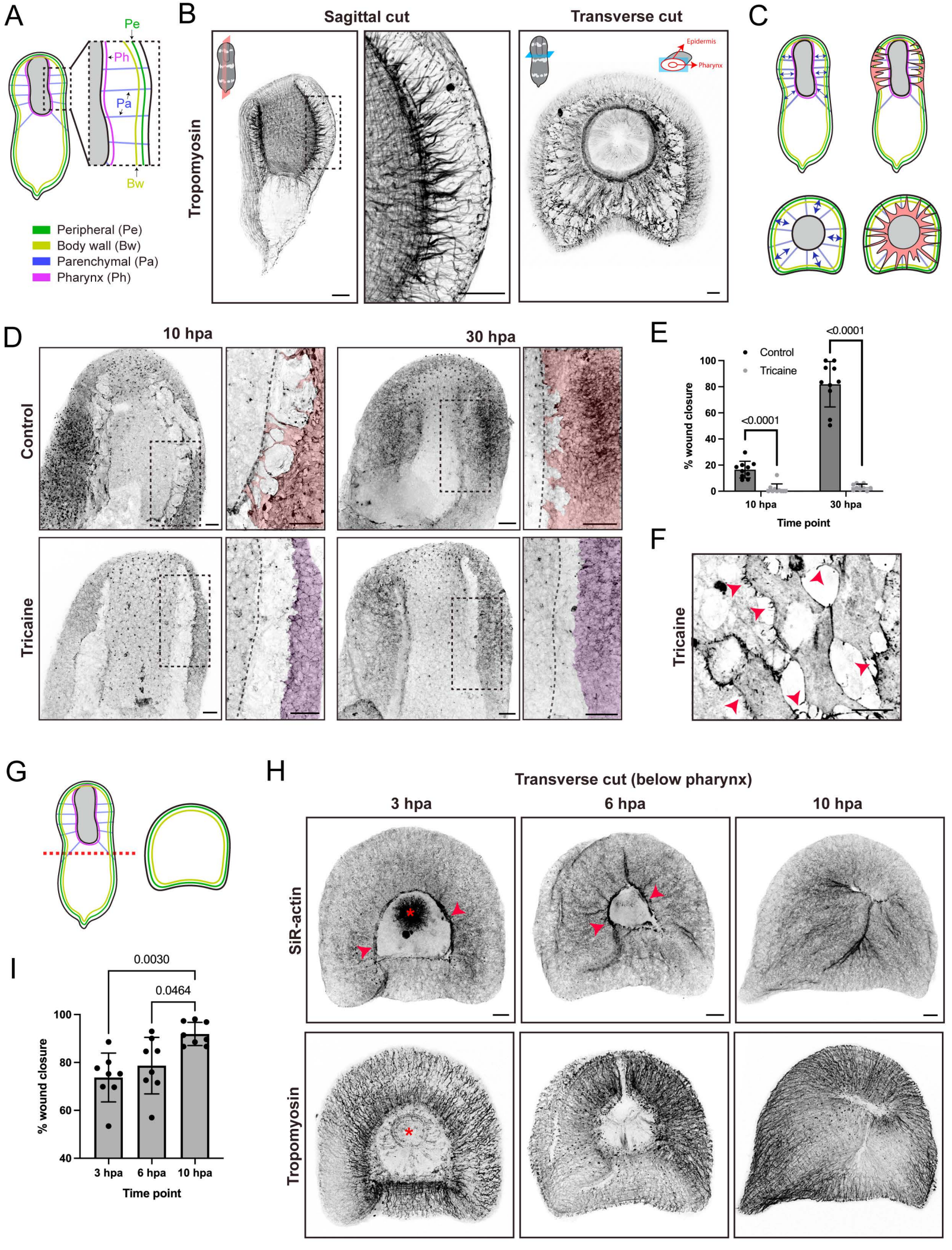
A
Pe
Ph
Pa
Bw
Peripheral (Pe)
Body wall (Bw)
Parenchymal (Pa)
Pharynx (Ph)
B
Sagittal cut
Transverse cut
Tropomyosin
Epidermis
Pharynx
C
D
10 hpa
30 hpa
Control
Tricaine
E
Control
Tricaine
% wound closure
<0.0001
<0.0001
10 hpa
30 hpa
Time point
F
Tricaine
G
H
Transverse cut (below pharynx)
3 hpa
6 hpa
10 hpa
SiR-actin
Tropomyosin
I
0.0030
0.0464
% wound closure
3 hpa
6 hpa
10 hpa
Time point